Proceedings of the 28th IEEE
EMBS Annual International Conference
New York City, USA, Aug 30-Sept 3, 2006

A Noncontact Measurement of Saccadic Eye Movement with Two High-speed Cameras

Akinori Ueno*, *Member, IEEE*, Yuji Otani, and Yoshinori Uchikawa, *Member, IEEE*

***Abstract*—A noncontact method for measuring saccadic eye movement with two high-speed cameras is proposed. The method is based on image processing for acquiring the center gravity of one pupil of the subject and also on stereo photogrammetry for estimating three-dimensional coordinate of the pupil. The proposed method was examined through experiments using a imitated eye ball and using a real human subject. The results showed a possibility of the method for the measurement. Since dynamic characteristics of the saccadic eye movement is reported as a promising index for monitoring human vigilance level according to the author's previous research works, this method can be utilized for accident prevention system in the future. However, there is still room for improvement in measuring accuracy and stability to the body motion in terms of its practical use.**

I. Introduction

THE increasing number of traffic accidents in Japan due to a diminished driver's vigilance level has become a problem of serious concern to the society. The driver with a diminished vigilance level suffers from a marked decline in his/her abilities of perception, recognition, and vehicle control. Therefore such driver poses serious danger to his/her own life and to the lives of other people. For this reason, it is essential to develop some systems that actively monitor drivers' level of vigilance and adaptively execute some actions for accident prevention such as feeding back monitored information to the driver, or alerting the driver of insecure driving condition, or switching to automatic slowing down.

On the other, the authors have focused on dynamic characteristics of saccadic eye movement (saccade: SC) as a candidate of vigilance index, and have investigated correlations between the characteristics of SC and vigilance indices that are assessed quantitatively from physiological, psychological, or psychophysical variables [1-7]. In the articles [1-5], spectral powers of EEG at Fz, Cz, and Pz during eye tracking task were analyzed, and were found to correlate closely with standardized peak velocity, standardized duration, and the ratio of peak velocity to duration (PV/D) of SC, respectively. In [4, 5], correlations with subjective sleepiness of Kwansei-Gaukin Sleepiness Scale (Japanese translation of Stanford Sleepiness Scale [8]) and with the score of self-rating in vigilance level were also investigated through 24-hour sleep deprivation experiment, and high correlations among the SC parameters and subjective indices were confirmed. Additionally, we have showed implications between the SC parameters and a newly devised performance index of visual perception [6, 7]. In view of our previous results and the fact that SC is the eye movement most frequently generated during driving as well as in our daily life, the dynamic characteristics of SC promise to be a sensitive and reliable index for monitoring driver's vigilance.

However, commonly available eye movement monitors are mostly head-coupled devices like goggle or glasses (f.e. ASL: Model 310, Takei Scientific Instruments: T.K.K.2901). Since it is not realistic to expect drivers to wear some dedicated devices on their head for doze prevention in daily driving, non-obtrusive and awareness-free monitor is strongly desired. A few devices allow remote measurement of eye direction, yet time resolution is not enough because SC needs a time resolution more than 500 Hz for accurate detection. With these backgrounds in mind, the authors have proposed a method for measuring SC remotely and constructed a stereo measurement system with 500 Hz high-speed cameras.

II. Algorithm for the Measurement

The proposed algorithm consists of three parts of (a) ocular image processing, (b) estimation of a three-dimensional (3D) coordinate of the center of gravity of the pupil, and (c) calculation of an eye rotation angle. Detail of each part is as follow. The all proposed algorithms are programmed by C++ language for validation of the algorithm.

A. Ocular Image Processing

Fig. 1 shows a flow chart of the ocular image processing. Monochrome ocular image sequences are acquired by two high-speed cameras with 8 bit grey scale at 500 Hz. Since pupil absorbs lights with wide range of light wavelength, hence appears darker than the other regions in the image, image binarization is applied to extract pupil region for each ocular image. When the grey scale of a scanned pixel is greater than a threshold, the grey scale of the pixel is changed to 255, and when smaller or equal to the threshold, the grey scale is set to 0. After the binarization, image denoising is

This work was addressed partially as a research sponsored by TOYOTA MOTOR Co. in 2002, 2003, and as part of the 21st Century COE (Center of Excellence) Research by the Ministry of Education, Culture, Sports, Science and Technology in 2004, 2005, and 2006.

*A. Ueno is with the Department of Electronic and Computer Engineering, Tokyo Denki University, Ishizaka, Hatoyama-machi, Saitama 350-0394, Japan (phone: +81-49-296-2911 ext.3147; fax: +81-49-296-6413; e-mail: ueno@f.dendai.ac.jp).

Y. Otani was with the Master's Program in Electronic and Computer Engineering, Tokyo Denki University, Saitama 350-0394, Japan.

Y. Uchikawa is with the Department of Electronic and Computer Engineering, Tokyo Denki University, Saitama 350-0394, Japan

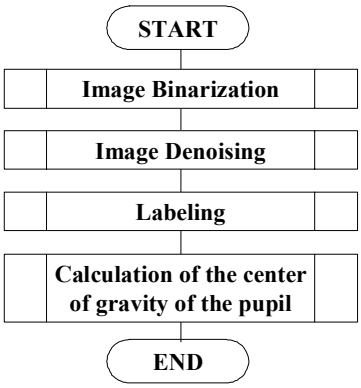

Fig. 1. A flow chart of the ocular image processing. The processing is applied to each image acquired from two high-speed cameras.

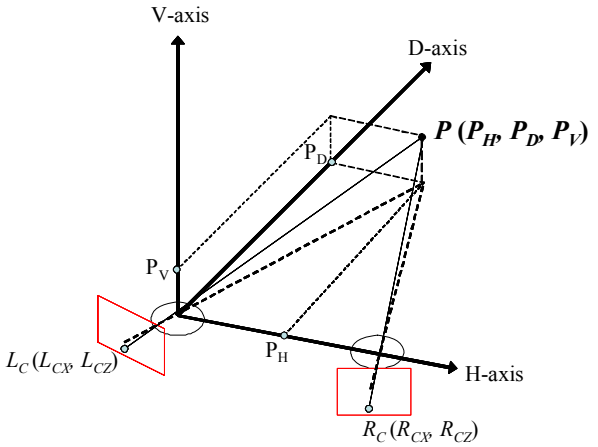

Fig. 2. A model coordinate system for estimating 3D position of the center of gravity of the pupil. Point P (P_H,,P_D,,P_V) in the figure represents the center of gravity to be assumed.

conducted twice for sure noise reduction. As a third step, every object composed of adjacent pixels is labeled with an integer from 1 to 254, and grey scales of all pixels consisting of an object are set to the labeled number. The object corresponding to the pupil is assumed to that composed of largest quantity of pixels. Finally, the centers of gravity R_C (R_{CX}, R_{CZ}) and L_C (L_{CX}, L_{CZ}) are calculated for both pupils detected from each image acquired by right and left cameras using the following equations:

$$(R_{cx}, R_{cz}) = \frac{1}{N_R}\sum_{i=1}^{N_R}(Rx_i, Rz_i) \quad \cdots\cdots (1)$$

$$(L_{cx}, L_{cz}) = \frac{1}{N_L}\sum_{j=1}^{N_L}(Lx_i, Lz_i) \quad \cdots\cdots (2)$$

where N_R and N_L are total number of pixels consisting of each pupil detected from right and left images, and (Rx_i, Rz_i) and (Lx_j, Lz_j) are ith or jth coordinate of the pixels respectively.

A. Estimation of Three-Dimensional Position of the Center of Gravity of the Pupil

Fig. 2 shows a model coordinate system for estimating three-dimensional (3D) position of the center of gravity of the pupil. Two ellipses in the figure indicate crystalline lenses in the right and left cameras respectively, and parallelograms behind the ellipses represent imaging areas in each camera. In this part, two-dimensional positions of the center of gravity of the pupil on the right and left imaging areas, that are calculated in previous section II-A as R_C (R_{CX}, R_{CZ}) and L_C (L_{CX}, L_{CZ}), are converted to a 3D position of P (P_H, P_D, P_V) expressed in the model coordinate system (Fig. 2). The original point of the system is defined as the center of the crystalline lens on the subject's left. The horizontal axis (H-axis) is defined by straight line passing through two centers of the right and left lenses.

The estimation of the 3D position is based on the stereo photogrammetry. In the first stage, P_H and P_D are estimated by using following equations:

$$(P_H, P_D) = \frac{L_{OO}\tan\beta}{\tan\alpha + \tan\beta}(1, \tan\alpha) \quad \cdots\cdots (3)$$

$$\alpha = \pi - \theta_L - \tan^{-1}\frac{B}{L_{CH}} \quad \cdots\cdots (4)$$

$$\beta = \pi - \theta_R - \tan^{-1}\frac{B}{R_{CH}} \quad \cdots\cdots (5)$$

$$L_{CH} = K_X\left(L_{CX} - \frac{XSIZE}{2}\right) \quad \cdots\cdots (6)$$

$$R_{CH} = K_X\left(R_{CX} - \frac{XSIZE}{2}\right) \quad \cdots\cdots (7)$$

where L_{OO} is distance between two centers of the lenses, and α and β are angles defined as $\alpha \equiv \angle P'OO_R$ and $\beta \equiv \angle P'O_RO$ respectively. O is the original point, O_R is the center of the crystalline lens on the subject's right, and P' is projected point of P on H-D plane. θ_L and θ_R are optic angles of the right and left cameras from H-axis. K_X is proportional constant in order to convert the unit of horizontal displacement from [pixel] to [mm], and $XSIZE$ is the number of pixels in crosswise (X) direction in imaging plane. And B is the distance between imaging planes and the center of the lens.

In the second stage, P_V is estimated by using following equations:

$$P_V = \frac{P_{VL} + P_{VR}}{2} \quad \cdots\cdots (8)$$

$$P_{VL} = \frac{L_{CV}\sqrt{P_H^2 + P_D^2}}{\sqrt{B^2 + L_{CH}}} \quad \cdots\cdots (9)$$

$$P_{VR} = \frac{R_{CV}\sqrt{P_H^2 + P_D^2}}{\sqrt{B^2 + R_{CH}}} \quad \cdots\cdots (10)$$

$$L_{CV} = K_Z\left(L_{CZ} - \frac{ZSIZE}{2}\right) \quad \cdots\cdots (11)$$

$$R_{CV} = K_Z\left(R_{CZ} - \frac{ZSIZE}{2}\right) \quad \cdots\cdots (12)$$

where K_Z is proportional constant to convert the unit of vertical displacement from [pixel] to [mm], and $ZSIZE$ is the number of pixels in longitudinal (Z) direction in imaging

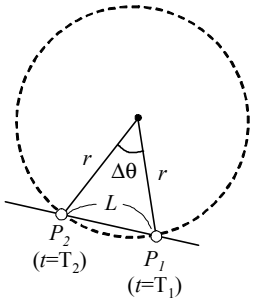

Fig. 3. Schematic diagram of estimation of ocular rotation angle in the H-D plane of the model coordinate system.

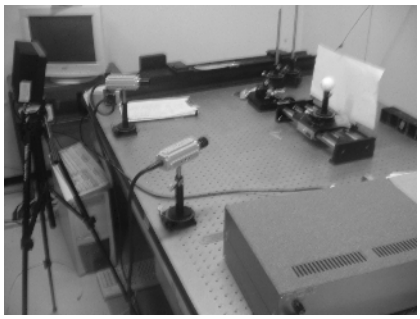

Fig. 4. Experimental setup for validation of the proposed algorithm using a imitated eyeball.

plane.

B. Estimation of the Ocular Rotation Angle

Rotation angle of the eye in the H-D plane of the model coordinate system is estimated from trajectory of the center of gravity of the pupil, which is assumed in the previous section II-B. Suppose a center of gravity of the pupil at t=T$_1$ [ms] is P_1 (P_{1H}, P_{1D}) and another at t=T$_2$ [ms] is P_2 (P_{2H}, P_{2D}), and radius of the rotation (i.e. approximately radius of the eyeball) is known to be r [mm] as shown in Fig.3, then angle difference $\Delta\theta_{1,2}$ between P_1 and P_2 can be calculated as follows:

$$L = \sqrt{(P_{1H} - P_{2H})^2 + (P_{1D} - P_{2D})^2} \quad \cdots\cdots (13)$$

$$\Delta\theta_{1,2} = 2\sin^{-1}\left(\frac{L}{2r}\right) \quad \cdots\cdots (14)$$

After the calculation, total rotation angle θ is computed by the summation of $\Delta\theta_{i,i+1}$, using the following equation:

$$\theta = \sum_{i=1}^{N-1} \Delta\theta_{i,i+1} \quad \cdots\cdots (15)$$

where N is the number of plot in the trajectory. Initial position of the processing is set to 0 deg. Counterclockwise rotation is assigned to positive rotation.

TABLE I
VALUES OF SYSTEM PARAMETERS USED IN THE EXPERIMENT

System Parameter	Parameter values for the experiment
L_{OO}	590 mm
Initial position of simulated eye ball	(292 mm, 547.2 mm)
K_X and K_Z	0.0102 mm/pixel
Focal length of the lenses	50 mm
Radius of the simulated eye ball	22.5 mm

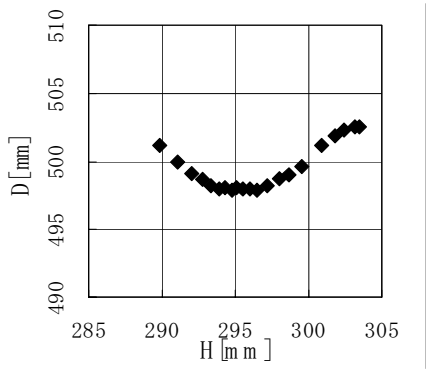

Fig. 5. Estimated trajectory of the centers of gravity of the pupil on the imitated eyeball, which was rotated from -20 deg to 20 deg by 2 deg in the H-D plane.

II. VALIDATION OF THE PROPOSED ALGORITHM USING A IMITATED EYEBALL

A. Experimental Method

Fig.4 shows experimental setup for validation of the proposed algorithm using a imitated eyeball. The setup was composed of two high-speed cameras with 500 Hz time resolution (Photoron, FASTCAM- PCI 500 2camera pack), a personal computer, and an infrared illuminator (American Dynamics, AD1020-6050). Infrared wavelength (880nm in the illuminator) was selected to gain high contrast between iris and pupil and to obtain clear image even while night driving. Two cameras were fixed on an optical bench (Sigma Koki, FB1612-50Y) using two θ axis rotation stages (Sigama Koki, KSP-786M) so that optic axes of the cameras were included in identical plane. Optic angles of θ_R and θ_L were set to 60 deg and 120 deg respectively. The imitated eye ball was fixed using also the θ axis rotation stage of the same model. Other system parameters used in the experiment are indicated in Table 1. The eye ball was rotated from -20 deg to +20 deg by 2 deg step in the H-D plane, and images of the eyeball were acquired through the high-speed camera at 500 Hz.

B. Results

Estimated coordinates of the center of gravity of the pupil on the imitated eyeball are shown in Fig. 5. As can be seen in Fig. 5, the estimated coordinates indicated a trajectory similar to circular arc. Fig. 6 is rotation angles calculated from the estimated coordinates in Fig. 5. As shown in Fig. 6, calculated rotation angles were nearly proportional to the theoretical

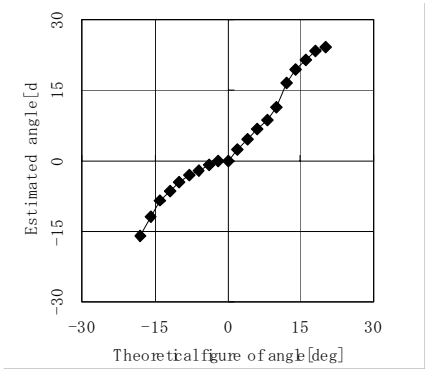

Fig. 6. Relation between theoretical figures and estimated results of eye rotation angle.

figures of the rotation angle.

III. Validation of the Algorithm with a Human Subject

A. Experimental Methods

The measurement system described in the section III-A was modified for the measurement with a human subject. Optic angles of θ_R and θ_L were set to 75 deg and 105 deg in this measurement. L_{OO} was set to 491.5mm, and initial distance in D-axis of the subject's eye P_D was 865 mm. Other parameter values were identical to the value in Table I. The subject was instructed to seat in front of and at the center between the 2 high-speed cameras so that the eye level of the subject becomes parallel to the H-D plane. Also the subject was requested to jump his eyes from a stationary target to the other target presented at 0deg and ±15deg. The measurement was conducted 8s at 500 Hz. The acquired images were processed by the proposed algorithm using the developed program.

B. Results

Fig. 7 shows time course variations in (a) estimated rotation angle and (b) estimated angular velocity of the center of gravity of the pupil. Successfully characteristic spikes corresponding to saccadic eye movement was confirmed in Fig. 7(b). These results infer that the proposed algorithm and constructed system are capable of detecting SC. However, estimated signal of the angular velocity is too noisy for extracting vigilance index of SC. Therefore, there is still room for improvement in terms of its practical use.

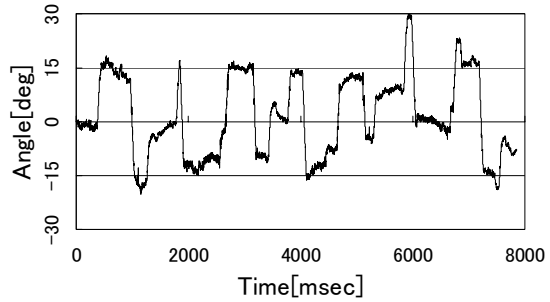

(a) Estimated angle

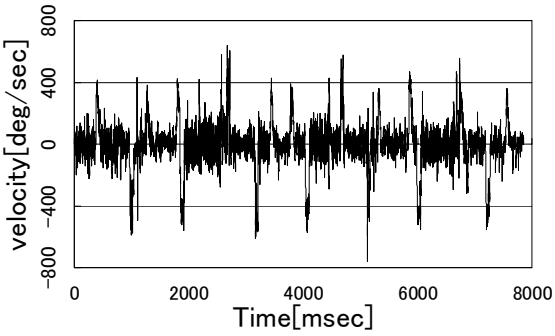

(b) Estimated angular velocity

Fig. 7. Time course variations in (a) estimated rotation angle and (b) estimated angular velocity of the subject.

IV. Conclusion

A noncontact method for measuring saccadic eye movement with two high-speed cameras is proposed, and a possibility of the proposed method for the measurement is confirmed through experiments using an imitated eye ball and using a human subject.

References

[1] A. Ueno, Y. Ota, M. Takase, and H. Minamitani, "Relationship between vigilance levels and characteristics of saccadic eye movement", *Proc. 17th Ann. Int. Conf. IEEE EMBS*, pp. 572-573, Sept. 1995.

[2] A. Ueno, Y. Ota, M. Takase, and H. Minamitani, "Characteristics of visually triggered and internally guided saccade depending on vigilance states," (in Japanese) *IEICE Trans. Information and Systems PT.2*, vol.J81-D-II, no.6, pp.1411-1420, June 1998.

[3] A. Ueno, Y. Ota, M. Takase, and H. Minamitani, "Parametric analysis of saccadic eye movement depending on vigilance states," *Proc. 18th Ann. Int. Conf. IEEE EMBS*, pp.319-320, Nov. 1996.

[4] A. Ueno, H. Hashimoto, M. Takase, and H. Minamitani, "Diurnal variation in vertical saccade dynamics," *Proc. 4th Asia-Pacific Conf. Medical and Biological Engineering*, p.373, Sept. 1999.

[5] A. Ueno, T. Tateyama, M. Takase, and H. Minamitani, "Dynamics of saccadic eye movement depending on diurnal variation in human alertness," *System and Computers in Japan*, vol.33, no.7, pp.95-103, June 2002.

[6] A. Ueno and Y. Uchikawa, "Relation between human alertness, velocity wave profile of saccade, and performance of visual activities," *Proc. 26th Ann. Int. Conf. IEEE EMBS*, pp.933-935, Sept. 2004.

[7] A. Ueno, S. Sakamoto, and Y. Uchikawa, "Relation between dynamics of saccade and bit rate for visual perception during numerical targets comparing," (in Japanese) *IEICE Trans. Information and Systems PT.2*, vol.J87-D-II, no.11, pp.2062-2070, Nov. 2004.

[8] J. Herscovitch and R. Broughton, "Sensitivity of the Stanford sleepiness scale to the effects of cumulative partial sleep deprivation and recovery oversleeping," *Sleep*, vol.4, no.1, pp.83-92, 1981.